INORGANIC CHEMISTRY
FRONTIERS

RESEARCH ARTICLE

View Article Online
View Journal | View Issue

Cite this: *Inorg. Chem. Front.*, 2024, **11**, 515

Magnetic exchange, anisotropy and excitonic fluctuations in a [Ni^{II}_7] Anderson wheel†

Emily H. Payne, [a] Lucinda R. B. Wilson, [a] Mukesh K. Singh, [a] Gary S. Nichol, [a] J. R. Stewart,[b] V. Garcia-Sakai, [b] R. A. Ewings,[b] Harry Lane,[c] Jürgen Schnack, *[d] Chris Stock*[c] and Euan K. Brechin *[a]

Received 8th November 2023,
Accepted 23rd November 2023

DOI: 10.1039/d3qi02307a

rsc.li/frontiers-inorganic

The solvothermal reaction of $Ni(ClO_4)_2{\cdot}6H_2O$ with hmpH and picH in a basic MeOH solution affords $[Ni_7(hmp)_{7.55}(pic)_{4.45}](ClO_4)_2{\cdot}6MeOH$ (**1**·6MeOH) directly upon cooling the mother liquor. The metallic skeleton of **1** describes a [Ni^{II}_7] centred hexagon, commonly referred to as an Anderson wheel. Magnetic measurements reveal ferromagnetic exchange between the central Ni ion and the ring Ni ions, and antiferromagnetic exchange between neighbouring ring Ni ions. They also confirm the presence of easy-plane anisotropy for the central Ni ion, and easy-axis anisotropy for the ring Ni ions, in agreement with DFT calculations and neutron scattering. For the analysis of the latter we apply an excitonic formalism using a Green's function response theory.

Introduction

Complexes of Ni^{II} have long played a prominent role in the field of molecular magnetism, from the early studies of magneto-structural correlations in Ni dimers[1] and cubes[2] and the emergence of Single-Molecule Magnets (SMMs),[3] to the design of molecules exhibiting very large magnetic anisotropies[4] and possessing long coherence times.[5] During this journey coordination chemists have developed a breadth of synthetic strategies in order to construct complexes with a variety of nuclearities and topologies. Amongst these, [Ni_4] SMMs have proven to be a particularly fruitful source of information on exchange bias effects,[6] antisymmetric exchange,[7] quantum tunnelling,[8] transverse anisotropy,[9] and Berry Phase interference.[10] Other common structural motifs demonstrating fascinating magnetic properties include wheels[11] and discs.[12] The latter offer interest from a variety of perspectives, including as molecular analogues of 2D lattices,[13] model complexes to examine spin frustration[14] and as robust platforms to quantitatively analyse magneto-structural correlations.[15]

Planar heptanuclear discs conforming to centred hexagons are often referred to as Anderson or Anderson-Evans wheels,[16] and are a common structure type in both polyoxometalate chemistry[17] and clusters of paramagnetic 3d ions.[18] A search of the Cambridge Structural Database (CSD) reveals that there are twenty nine [Ni^{II}_7] Anderson wheels.[19–38] Of these, fifteen have had their magnetic behaviour reported, but only five have been subject to quantitative analysis.[21,26,30,36,37] This is perhaps not surprising. Given the potential for multiple (≤12) exchange interactions, and numerous g and D values, even greatly simplified models can prove computationally demanding. In general, extracting exchange coupling constants (J) has been achieved using a model which assumes just two interactions (Fig. 1), one between the central Ni ion and the Ni ions in the outer ring (J_{cr}) and one between neighbouring Ni ions around the ring (J_{rr}). However, there is no agreement regarding the nature and magnitude of these values for those complexes exhibiting competing ferro- and antiferromagnetic exchange, despite the presence of similar Ni–X–Ni angles. Some reports suggest J_{cr} is ferromagnetic and J_{rr} is antiferromagnetic, and others state J_{cr} is antiferromagnetic and J_{rr} is ferromagnetic. The only clear-cut case is when all bridges are $\mu_{2/3}$-N_3^- ions which promote ferromagnetic exchange for both J_{cr} and J_{rr}.[30] Based on magneto-structural correlations developed for [Ni_4O_4] cubanes,[2] one might expect J_{cr} to be ferromagnetic and J_{rr} antiferromagnetic in all O-bridged species given that the former are mediated by μ_3-O atoms with smaller Ni–O–Ni angles than the latter, which are bridged by μ_2-O atoms. Indeed, this is what is observed in a [$Al^{III}_2Ni^{II}_5$] Anderson wheel reported recently, where J_{cr} = +10 cm^{-1} and J_{rr} = −5 cm^{-1} ($\hat{H} = -2\sum_{i<j} J_{ij}\hat{\vec{s}}_i \cdot \hat{\vec{s}}_j$ formalism).[15] There is also no agreement on

[a]*EaStCHEM School of Chemistry, The University of Edinburgh, David Brewster Road, Edinburgh, EH9 3FJ Scotland, UK. E-mail: E.Brechin@ed.ac.uk*
[b]*ISIS Pulsed Neutron and Muon Source, STF Rutherford Appleton Laboratory, Harwell Campus, Didcot, Oxon, OX11 0QX, UK*
[c]*School of Physics and Astronomy, The University of Edinburgh, Edinburgh, EH9 3JZ Scotland, UK. E-mail: C.Stock@ed.ac.uk*
[d]*Fakultät für Physik, Universität Bielefeld, Postfach 100131, D-33501 Bielefeld, Germany. E-mail: jschnack@uni-bielefeld.de*

†Electronic supplementary information (ESI) available. CCDC 2286832. For ESI and crystallographic data in CIF or other electronic format see DOI: https://doi.org/10.1039/d3qi02307a

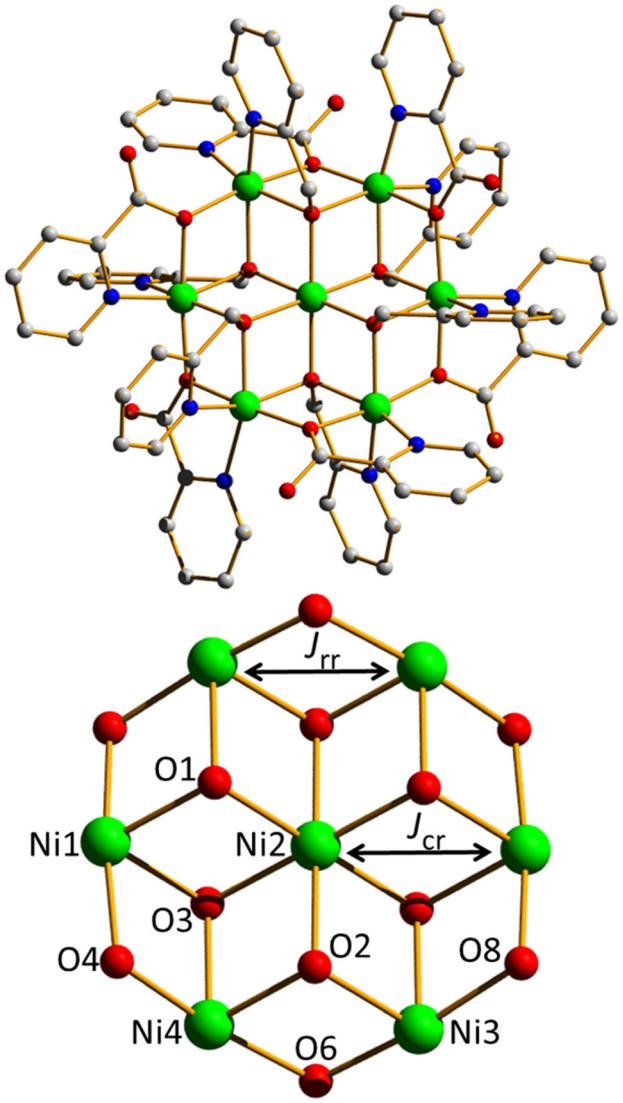

Fig. 1 Molecular structure of the cation of complex **1** (top). The metal–oxygen core of complex **1** (common to the majority of Anderson wheels) alongside the two exchange interactions (J_{cr} and J_{rr}; c = centre, r = ring) most often employed to describe the magnetic exchange interactions present (bottom). Colour code: Ni = green, O = red, N = blue, C = grey. H atoms, counter anions and solvent of crystallisation omitted for clarity.

the sign and magnitude of the zero-field splitting (D_{Ni}) for the central or ring Ni^{II} ions. In order to investigate the magneto-structural relationship in this family of complexes further, and to unequivocally extract the relevant spin-Hamiltonian parameters, we have synthesised and characterised the complex $[Ni_7(hmp)_{7.55}(pic)_{4.45}](ClO_4)_2$·6MeOH (**1**·6MeOH; Fig. 1, hmpH = 2-(hydroxymethyl)pyridine, picH = picolinic acid) using a combination of susceptibility and magnetisation measurements, magnetic neutron spectroscopy and first principles calculations. This complementary trio of techniques, employed for the first time in the analysis of [Ni_7] Anderson wheels, reveals the presence of competing ferro- and antiferromagnetic exchange interactions and both easy plane and easy axis anisotropy.

Experimental

Experimental procedures

All chemicals were procured from commercial suppliers and used as received (reagent grade).

Synthesis of $[Ni_7(hmp)_{7.55}(pic)_{4.45}](ClO_4)_2$·6MeOH (1·6MeOH)

$Ni(ClO_4)_2·6H_2O$ (0.366 g, 1 mmol) was dissolved in MeOH (20 mL), with NaOMe (0.162 g, 3 mmol) yielding a pale blue solution. To this, hmpH (0.142 mL, 1.5 mmol) was added dropwise followed by picH (0.184 g, 1.5 mmol), which resulted in a deep blue solution. The solution was stirred for 12 hours and then transferred to a Teflon-lined, stainless steel autoclave which was heated for 24 hours at 140 °C. This was then allowed to cool for a further 24 hours, yielding translucent pale blue plate-shaped crystals. Anal. calcd (%) C, 43.91; H, 3.23; N, 8.54. Found: C, 43.81; H, 3.39; N, 8.49. Yield: 56%.
Note: caution should be taken when using/heating the potentially explosive perchlorate anion.

Crystallographic details

A suitable crystal with dimensions 0.48 × 0.14 × 0.04 mm^3 was selected and mounted on a MITIGEN holder in Paratone oil on a Rigaku Oxford Diffraction XCalibur diffractometer. The crystal was kept at a steady T = 120.0 K during data collection. The structure was solved with the ShelXT solution program using dual methods, employing Olex2 as the graphical interface. The model was refined with ShelXL 2018/3 using full matrix least squares minimisation on F^2.[39–41] Three of the ligands were modelled as a disordered mixture of hmp and pic, as evidenced by a residual peak in a difference map which corresponded to the additional O site in the pic ligand. Each disorder was refined with a separate free variable. Specific occupancy values are given in the CIF; this explains the fractional values in the formula. Other than constructing an appropriate disorder model for the CH_2 group the ring atoms of each hmp/pic disorder were not split as this was not justified by either the displacement ellipsoids or residual electron density peaks.

Crystal data. $C_{78}H_{87.09}Cl_2N_{12}Ni_7O_{30.45}$, M_r = 2161.75, triclinic, $P\bar{1}$ (No. 2), a = 12.1951(3) Å, b = 13.4801(4) Å, c = 15.0616 (4) Å, α = 110.946(3)°, β = 97.395(2)°, γ = 106.809(2)°, V = 2137.68(10) $Å^3$, T = 120.0 K, Z = 1, Z' = 0.5, μ(MoKα) = 1.662, 57 226 reflections measured, 10 646 unique (R_{int} = 0.0441) which were used in all calculations. The final wR_2 was 0.1078 (all data) and R_1 was 0.0465 ($I \geq 2\sigma(I)$). CCDC 2286832.† Powder XRD data of compound **1** (Fig. S1†) were collected on a polycrystalline powder using a Bruker D8 ADVANCE in transmission mode fitted with a LynxEye detector using Cu radiation at 40 kV, 40 mA and a Johansson monochromator, 2 mm divergence slit and 2.5° Soller slits on the incident beam side. Bruker's DIFFRAC software was used to control the diffractometer. Diffraction data were measured from 2θ = 5°–40°; step size, 0.0101°.

Magnetic thermodynamic measurements

Magnetic susceptibility and magnetisation measurements were performed on a powdered crystalline sample restrained in eicosane in the temperature and fields ranges T = 2–300 K, B = 0.1 T and T = 2–6 K, B = 0.5–7.0 T, respectively, using a Quantum Design MPMS XL SQUID magnetometer equipped with a 7 T dc magnet. The observed paramagnetic susceptibilities were corrected for diamagnetic contributions using Pascal's constants.

Computational details

Density Functional Theory (DFT) calculations in the Gaussian16 suite[42] have been performed to estimate the magnetic exchange interactions between the Ni^{II} centres on a $[Ni_5Zn_2]$ model, constructed by replacing two Ni^{II} ions with two Zn^{II} ions (Fig. S2a and b†) in the XRD structure of complex **1**. The hybrid B3LYP functional[43] together with the TZV basis set[44] have been employed for the Ni and Zn atoms, the 6-31G* basis set has been used for the O and N atoms, while the 6-31G basis set has used for the C and H atoms.[45] Noodleman's broken symmetry approach[46] has been employed for estimating the magnetic exchange interactions. Spin configurations used to estimate the exchange coupling constants are summarised in Table S1.† Pairwise interactions have been calculated to estimate the magnetic interaction between (a) the central Ni^{II} ion and the outer ring Ni^{II} ions (J_{cr}), and (b) between the ring Ni^{II} ions (J_{rr}), in dimeric models **1A–1B** (Fig. S2c and d†), respectively. We have also developed magneto-structural correlations on model **1C** (Fig. S2e†) to check the dependence of the magnetic exchange interaction on the average Ni–O distance and average Ni–O–Ni angle. We have made several mono- and dimetallic models (**1D–1G**, Fig. S2f–i†) from complex **1** to estimate the zero field splitting parameters for each Ni^{II} centre using the ORCA software suite (version ORCA 4.0).[47] The zeroth-order regular approximation (ZORA) method together with the ZORA contracted version of the basis set (ZORA-def2-TZVP for Ni, Zn and ZORA-def2-SVP for rest of the elements) have been used. The calculation further utilised the resolution of identity (RI) approximation with the auxiliary def2-TZVP and def2-SVP Coulomb fitting basis sets.[48] During state-average complete active space self-consistent field (SA-CASSCF) calculations, we have included eight electrons in five d-orbitals (CAS (8 electrons/5 3d-orbitals)) in the active space. Ten triplet and fifteen singlet roots are considered during CASSCF calculations. To consider the dynamic correlation, we have performed 2^{nd} order N-electron valence perturbation theory (NEVPT2) calculations.[49] We have employed integration Grid 6 for the Ni and Zn ions, and Grid 5 for remaining elements.

Neutron spectroscopy, data correction and background subtraction

Neutron spectroscopy measurements were performed on the LET (ISIS, Didcot) cold chopper spectrometer. The sample was fully protonated for these measurements, resulting in a large background from the incoherent cross section from H-atoms, as discussed below. Given the large amount of neutron incoherent scattering resulting from H and Ni, there was a significant temperature independent background in the spectroscopic data taken on LET. This primarily originated from elastic scattering leaking into inelastic channels due to instrumental effects such as finite resolution. To account for this, we have applied the principle of detailed balance to remove this background, following previous scattering studies where this has been successfully used.[50] This analysis depends on the fact that at a fixed momentum and energy transfer, the measured intensities at the neutron energy gain (negative energy transfer) and energy loss (positive energy transfer) are related by the following expression with the energy transfer defined as $E \equiv \hbar\omega = E_i - E_f$

$$\begin{aligned} I_{meas}(+|E|, T) &= B_1(+|E|) + S(|E|, T) \\ I_{mes}(-|E|, T) &= B_2(-|E|) + S(|E|, T)e^{-E/kT} \end{aligned} \quad (1)$$

where B_1 and B_2 are temperature-independent background constants for positive and negative energy transfers. $S(|E|, T)$ is proportional to the structure factor which contains both lattice and magnetic contributions. Note that ± energies are related through the $e^{-E/kT}$ term which is the Boltzmann factor. An assumption in this analysis is that the resolution function does not change substantially over the energy range of interest and therefore the measured intensities at $\pm|E|$ are related solely by detailed balance.

In our experiment on LET, data were collected at four different temperatures, T = 2, 20, 50, and 80 K. With data at $\pm|E|$ at each temperature, this gives eight data points for a given momentum Q and energy transfer $|E|$. Assuming temperature independent background parameters of B_1 and B_2 and four values of $S(|E|, T$ = 2, 20, 50, and 80 K), this is a closed problem of fitting six parameters to eight data points for each momentum and energy transfer. To obtain the temperature independent background we performed a least-squares fit to each Q and $|E|$ to obtain the temperature independent background parameters $B_{1,2}$. We then used this to subtract off the background from the data, leaving the structure factor $S(|E|, T)$ which can be computed theoretically and compared to first principle calculations as discussed below.

Results and discussion

Synthesis and structure

The solvothermal reaction of $Ni(ClO_4)_2{\cdot}6H_2O$ with hmpH and picH in a basic MeOH solution affords blue plate shaped crystals of formula $[Ni_7(hmp)_{7.55}(pic)_{4.45}](ClO_4)_2{\cdot}6MeOH$ (**1**·6MeOH) directly upon cooling the mother liquor. The crystals were found to be in a triclinic cell and structure solution was carried out in the space group $P\bar{1}$. The asymmetric unit (ASU) comprises half of the formula. The metallic skeleton describes a $[Ni^{II}_7]$ centred hexagon, commonly referred to as an Anderson wheel. The central Ni ion is connected to the six

ring Ni ions through a total of six μ_3-O atoms deriving from the hmp ligands with Ni–O–Ni angles in range ~96.4–99.0°. These O-atoms also provide the connectivity between neighbouring Ni ions around the inner rim of the [Ni^{II}_6] ring with Ni–O–Ni angles in the range ~97.2–98.4°. The outer rim of the ring is connected by six μ_2-O atoms derived from the pic ligands with Ni–O–Ni angles in range ~100.3–100.5°. Note the latter are larger than the former. All six Ni^{II} ions are six-coordinate and in distorted octahedral geometries. The central Ni^{II} ion possesses a {NiO_6} coordination sphere, while those in the ring are {NiO_4N_2}. Note that the hmp/pic disorder in three of the organic ligands, as described in the crystallography details section, has no effect upon the Ni coordination spheres. The two ClO_4 anions sit above and below the [Ni_7] plane, with the MeOH molecules of crystallisation H-bonded to the non-bonded O-arm of the pic ligands (O···(H)O, ~2.75–2.81 Å). In the extended structure this leads to a brickwork-like arrangement of cluster cations. The closest intermolecular Ni···Ni distances are >7.7 Å.

Dc magnetic susceptibility and magnetisation measurements

Dc magnetic susceptibility (χ) and magnetisation (M) measurements were performed on a powdered microcrystalline sample of **1** in the T = 300–2 K, B = 0.1 T and T = 2–6 K, B = 0.5–7.0 T ranges, respectively. These data are shown in Fig. 2 (and Fig. S3†) in the form of the χT product *versus* T and M *vs.* B. The χT product at T = 300 K is 8.6 cm^3 K mol^{-1}, similar to the Curie constant expected for seven uncorrelated S = 1 ions with g = 2.2 (8.5 cm^3 K mol^{-1}). As temperature decreases the χT product slowly increases to a maximum value of 12.0 cm^3 K mol^{-1} at T = 20 K, before decreasing at lower temperatures to a value of 10.5 cm^3 K mol^{-1} at T = 2.0 K. The magnetisation data initially increase rapidly with increasing magnetic field (M = 7μ_B at B = 1 T and T = 2 K) T and then rise more gradually thereafter to a maximum value of M = 11μ_B at B = 7 T and T = 2 K. The susceptibility and magnetisation data are therefore indicative of the presence of both ferro- and antiferromagnetic exchange interactions. The susceptibility data can be simulated nicely (Fig. S3†) with an isotropic spin-Hamiltonian $\hat{H} = -2\sum_{i<j} J_{ij}\hat{\vec{s}}_i \cdot \hat{\vec{s}}_j$ to a model that assumes just two independent exchange interactions, J_{cr} and J_{rr}, describing the interaction between the central Ni ion and ring Ni ions, and between ring Ni ions, respectively.

The fit can be improved by adding additional J_{cr} and J_{rr} interactions (J_1–J_4, Fig. S3†), permitted given the presence of just inversion symmetry in **1** (*i.e.* half the cluster is in the ASU). In all cases the J_{cr} interaction is found to be ferromagnetic and the J_{rr} interaction is found to be antiferromagnetic. However, this simple isotropic model does not fit the magnetization data in the full temperature and field range, particularly at high fields. Introduction of an anisotropic term $\hat{H} = \sum_i D_i(\hat{S}_i^z)^2$ to account for the zero-field splitting associated with the octahedral Ni^{II} ions is therefore required, one for the central Ni ion with an {NiO_6} coordination sphere (D_1) and one for the ring Ni ions with {NiO_4N_2} coordination spheres (D_2). The best fit of the susceptibility and magnetisation data with this model affords J_1 = +4.13 cm^{-1}, J_2 = −4.20 cm^{-1}, J_3 = +3.93 cm^{-1}, J_4 = −0.80 cm^{-1}, D_1 = +4.71 cm^{-1} and D_2 = −3.02 cm^{-1}. Note the opposite signs of D_1 and D_2, positive for the central Ni^{II} ion and negative for the ring Ni^{II} ions.

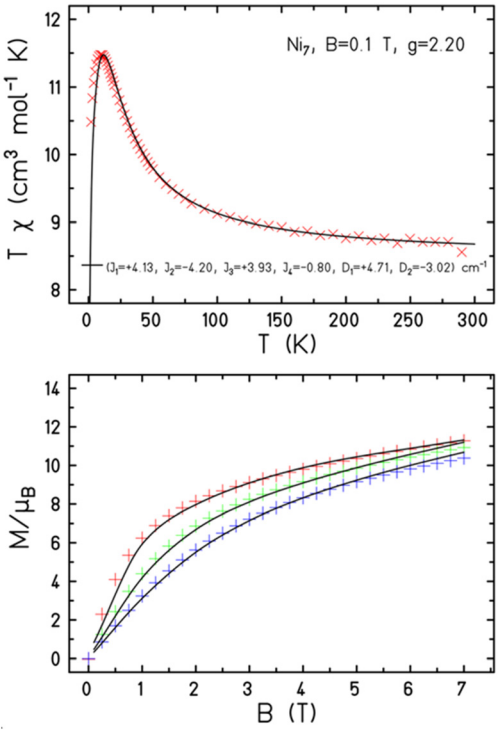

Fig. 2 Plot of the χT product *vs.* T (top) and M *vs.* B (bottom) for **1**. The solid lines are a fit of the data to the model described in the text and Fig. S3.† J_1, J_3 = J_{cr}, J_2, J_4 = J_{rr}, D_1 = zfs of central Ni, D_2 = zfs of ring Ni. In the lower panel T = 2 K (+), T = 4 K (+), T = 6 K (+). The best fit is for J_1 = +4.13 cm^{-1}, J_2 = −4.20 cm^{-1}, J_3 = +3.93 cm^{-1}, J_4 = −0.80 cm^{-1}, D_1 = +4.71 cm^{-1}, D_2 = −4.02 cm^{-1}. Uncertainties are estimated as 0.1–0.2 cm^{-1}.

DFT calculations

To further support the sign and magnitude of the experimentally determined magnetic exchange interactions above, DFT calculations have been performed on a [Ni_5Zn_2] model created from the XRD structure of complex **1** (Fig. S2a and Table S1†). Considering symmetry and structural parameters, complex **1** has a total of five unique magnetic exchange interactions (J_1 – J_4, $J_{1'}$ Fig. S2b†). The exchange between the central and ring Ni^{II} ions (J_{cr} = J_1, $J_{1'}$, J_3) is calculated to be ferromagnetic and in the range +3.1 cm^{-1} ≤ J_{cr} ≤ +5.1 cm^{-1}. The exchange between neighbouring ring Ni^{II} ions (J_{rr} = J_2, J_4) is calculated to be antiferromagnetic and in the range −1.6 cm^{-1} ≤ J_{rr} ≤ −6.0 cm^{-1}. Thus, the signs and magnitudes of the DFT calculated values are in good agreement with the experimentally fitted values derived from the magnetic susceptibility and magnetisation measurements. They are also in agreement with previous magneto-structural studies per-

formed on polymetallic Ni^{II} complexes in which larger average Ni–O–Ni angles result in an antiferromagnetic interaction and smaller average Ni–O–Ni angles result in a ferromagnetic interaction, with the crossover angle being ~97–98°.[1,2,15,51] Further DFT calculations on dimetallic models (Fig. S2c and d†) also confirm the ferromagnetic J_{cr} interaction (J_{1A} = +8.2 cm^{-1}) and antiferromagnetic J_{rr} interaction (J_{1B} = −3.1 cm^{-1}).

To rationalise the magnitude and sign of the magnetic interactions, overlap integral calculations[52] have been performed on the dimetallic models using the singly occupied molecular orbitals (SOMOs) of the Ni^{II} ions. Stronger overlap values between SOMOs leads to an antiferromagnetic interaction, whereas orthogonal/weak overlap values contribute to a ferromagnetic interaction. The overlap integral calculations suggest one moderate and three weak interactions for **1A** and two moderate and two weak interactions for **1B**. This leads to a ferromagnetic interaction for **1A** and an antiferromagnetic interaction for **1B** (Fig. S4 and 5†). Spin density analysis suggests strong mixing and delocalisation onto the coordinating ligand atoms followed by weak spin polarisation. The ring Ni^{II} ions have a spin density between 1.693–1.698 and the central Ni^{II} ion has a spin density of 1.735 (Fig. S6 and 7†). The smaller spin densities on the ring Ni^{II} ions can be attributed to the stronger spin delocalisation from the Ni^{II} ion to the N atom of the bridging ligand (between 0.050–0.063). As expected, the μ_3-O bridging atoms have a larger spin density compared to the μ_2-O bridging atoms.[51] A magneto-structural correlation developed for model **1C** (Fig. S2e†) with respect to the average Ni–O–Ni angle and average Ni–O distance follows the same trends observed for previously published O-bridged polymetallic Ni^{II} complexes, suggesting a strong dependence of the magnetic exchange interaction on the average Ni–O–Ni angle in particular (Fig. S8†).[51]

SHAPE analysis (Table S2†) suggests distorted octahedral geometries for all the Ni^{II} ions present, with the ring Ni^{II} ions [NiO_4N_2] being more distorted than the central Ni^{II} ion [NiO_6] on account of the chelating hmp/pic ligands. For small distortions away from ideal O_h symmetry, as seen here, one would expect either easy axis or easy plane anisotropy with a magnitude of approximately $|D|$ < 10 cm^{-1}.[52] Single ion anisotropy parameters for the four unique Ni^{II} ions present in **1** have been estimated using *ab initio* CASSCF/NEVPT2 calculations in the ORCA suite on model complexes **1D–1G** (Fig. S2f–i†) derived from the XRD structure of complex **1**.[47] *Ab initio* NEPVT2 calculations suggest easy axis anisotropy for the ring Ni^{II} ions in the range −5.4 $cm^{-1} \leq D_2 \leq$ −7.7 cm^{-1}, and easy plane anisotropy, D_1 = +7.3 cm^{-1}, for the central Ni^{II} ion (Fig. S9 and Table S3†). The D_{zz} axes for Ni1–3 lie along the shortest Ni-μ_3O distance, whereas for Ni4, D_{zz} is oriented along the longest Ni-μ_3O distance (Fig. S10†). The negative and positive signs of D are thus associated with the compressed and elongated character of the octahedron, respectively.[52] The calculated values are in agreement with the experimentally fitted values from the susceptibility and magnetization data, and consistent with values in the literature.[52] The ground state electronic arrangements for the ring and the central Ni^{II} ions are found to be $\{(d_{yz})^2\ (d_{xz})^2\ (d_{xy})^2\ (d_{z^2})^1(d_{x^2-y^2})^1\}$ and $\{(d_{yz})^2(d_{xy})^2(d_{xz})^2(d_{z^2})^1(d_{x^2-y^2})^1\}$ with the dominant spin conserved electronic transitions $d_{xy} \rightarrow d_{x^2-y^2}$ and $d_{xz} \rightarrow d_{x^2-y^2}/d_{z^2}$, respectively.

Excitonic magnetism

Above, a series of first principle calculations have been outlined producing a quantitative range for model parameters in the magnetic Hamiltonian of [Ni_7]. In this section we validate these parameters through a comparison with magnetic neutron scattering data. We first discuss the definition of the structure factor in terms of correlations of magnetic spins. We then discuss a formalism to calculate this dynamic structure applying Green's functions formalism that links the measured neutron scattering cross section with mean field response theory. We then consider the magnetic Hamiltonian of [Ni_7] and use this formalism to solve the case of an isolated [Ni_7] molecule for both the excitation energy levels and their corresponding neutron intensities determined by dipolar selection rules. The intensity measured in an experiment of scattering neutrons off magnetic Ni^{II} ions is directly proportional to the structure factor $S(\vec{Q},\omega)$,

$$S(\vec{Q},\omega) = g_L^2 f^2(Q) \sum_{\alpha\beta} (\delta_{\alpha\beta} - \hat{Q}_\alpha \hat{Q}_\beta) S^{\alpha\beta}(\vec{Q},\omega)$$

where g_L is the Landé factor and $f(Q)$ is the Ni^{II} form factor. The term $(\delta_{\alpha\beta} - \hat{Q}_\alpha \hat{Q}_\beta)$ is the polarization factor, reflecting the fact that neutron scattering is only sensitive to the spin component perpendicular to the momentum transfer, $\vec{Q}$. $S^{\alpha\beta}(\vec{Q},\omega)$ is the dynamic structure factor which is the Fourier transform of the spin–spin correlation function:

$$S^{\alpha\beta}(\vec{Q},\omega) = \frac{1}{2\pi} \int dt\, e^{i\omega t} \langle \hat{S}^\alpha(\vec{Q},t) \hat{S}^\beta(-\vec{Q},0) \rangle$$

where α, β = +,−, z. The dynamic structure factor $S^{\alpha\beta}(\vec{Q},\omega)$ is related to the Green's response function $G^{\alpha\beta}(\vec{Q},\omega)$ by

$$S^{\alpha\beta}(\vec{Q},\omega) = -\frac{1}{\pi} \frac{1}{1 - \exp(-\omega/k_B T)} Im(G^{\alpha\beta}(\vec{Q},\omega))$$

To relate the Greens function to the microscopic magnetic Hamiltonian, we note that in linear response theory, it is related to the Fourier transform of the retarded Green's function that is given by

$$G^{\alpha\beta}(ij,t) = -i\Theta(t) \langle [\hat{S}_i^\alpha(t), \hat{S}_j^\beta(0)] \rangle$$

with ij representing site indices with the heaviside function $\Theta(t)$ forcing causality by excluding negative values of t. By taking time derivatives of both sides of the equation and Fourier transforming, an equation of motion for the Green's function can be developed and hence related directly back to the neutron scattering cross section by taking the imaginary part, as outlined in previous studies.[53–56]

The approach followed in previous works[57] applying the Green's functions to neutron spectroscopy is to divide the magnetic Hamiltonian into two parts – a local single-ion part

for the magnetic ion of interest (including terms like the crystalline electric field, spin–orbit coupling, and molecular fields), and an interion part describing interaction between magnetic ions (usually modelled in terms of a Heisenberg exchange). Here, we simplify this by considering **1** as a single ion entity with the eigenstates of the total magnetic Hamiltonian defined by $\{|n\rangle\}$ with corresponding energy eigenvalues $\{\omega_n\}$. The Green's function is then reduced to the single-ion term,

$$G^{\alpha\beta}(\vec{Q},\omega) \equiv g^{\alpha\beta}(\omega) = \sum_{mn} \frac{S_{\alpha mn} S_{\beta nm}(f_m - f_n)}{\omega - \omega_n + \omega_m}$$

where the matrix elements are defined by $S_{\alpha mn} \equiv \langle m|S_\alpha|n\rangle$ and the thermal Boltzmann factors $f_n \equiv e^{-\omega_n/k_B T} / \sum_m e^{-\omega_m/k_B T}$. For calculation purposes, we set $\hbar\omega = E + i\Gamma$ where Γ can be physically interpreted as an energy broadening (or dampening) of the magnetic excitations sampled at an energy transfer of E. The final neutron cross section is then derived summing over all combinations of $g^{\alpha\beta}(\omega)$. Note that in the low temperature $T \to 0$ limit, this reduces to the simplified expression,

$$g^{\alpha\beta}(\omega) = \sum_n \left(\frac{S^\alpha_{0n} S^\beta_{n0}}{\omega - \omega_{n0}} - \frac{S^\alpha_{n0} S^\beta_{0n}}{\omega + \omega_{n0}} \right)$$

where $\omega_{n0} \equiv \omega_n - \omega_0$. This reduced expression avoids the need to sum over thermally excited inter-level transitions. The problem of calculating the neutron cross section then reduces to deriving the single ion response for **1**. Given that each Ni^{II} ion is in a $S = 1$ state, from Hund's rules and the Pauli principle, each of the seven Ni^{II} sites have a three-fold multiplicity associated with different z-axis projections. This results in **1** having $3^7 = 2187$ basis states. In this study, we have used these 2187 basis states to solve the following magnetic Hamiltonian exactly,

$$\mathcal{H} = H_{rr} + H_{CR} + H_{aniso}$$

with H_{rr}, H_{CR}, H_{aniso} corresponding to ring, central, and anisotropic terms of the magnetic Hamiltonian. The Ni^{II} labelling and notation is schematically illustrated in Fig. S11.† These are explicitly given by,

$$H_{rr} = J_{rr} \times \left[\vec{S}_1 \cdot \vec{S}_2 + \vec{S}_2 \cdot \vec{S}_3 + \vec{S}_3 \cdot \vec{S}_4 + \vec{S}_4 \cdot \vec{S}_5 + \vec{S}_5 \cdot \vec{S}_6\right]$$

$$H_{CR} = J_{CR} \times \left[\vec{S}_1 \cdot \vec{S}_7 + \vec{S}_2 \cdot \vec{S}_7 + \vec{S}_3 \cdot \vec{S}_7 + \vec{S}_4 \cdot \vec{S}_7 + \vec{S}_5 \cdot \vec{S}_7 + \vec{S}_6 \cdot \vec{S}_7\right]$$

$$H_{aniso} = D_2 \sum_{t=1}^{6} (S_t^z)^2 + D_1[(S_7^x)^2 + (S_7^y)^2]$$

where the indices 1–6 refer to the Ni^{II} ions on the ring and 7 the central Ni^{II} ion. This magnetic Hamiltonian divides up **1** into a problem with two exchange constants, J_{rr} and J_{CR}, and two anisotropic terms, $D_{1,2}$. Here we have used the result above that the spins on the outer wheel have uniaxial anisotropy while the inner spin has easy-plane anisotropy. Note that in the analysis discussed below, we have performed a fit without anisotropy, however this produces exchange constants that are unphysically large (for example $J_{CR} \sim -4$ meV $= -32$ cm^{-1}) in comparison to the first principles calculations and experimental fits discussed above. To constrain the parameters used to describe the neutron response, it is important to consider the magnetic susceptibility which is related to the real part of the Green's response function and to the imaginary part *via* Kramers–Kronig relations.

$$\chi = -g^2\mu_B^2 \lim_{\omega\to 0} Re\ g(\omega) = -\frac{g^2\mu_B^2}{\pi} \int d\omega \frac{Img(\omega)}{\omega}$$

In the high temperature paramagnetic limit the susceptibility scales as $\chi \propto 1/(T - \Theta_{CW})$. In mean field theory, a plot of χ^{-1} as a function of temperature has an x-axis intercept defined by the Curie–Weiss temperature, Θ_{CW}, and is related to the exchange constants by,

$$\Theta_{CW} = \frac{2}{3} S(S+1) \times 6(J_r + J_c)$$

which provides a way of constraining the Heisenberg exchange through fitting the high temperature susceptibility. Fig. S12† plots the inverse of the magnetic susceptibility where a fit of the data for $T > 100$ K (in the high temperature paramagnetic regime) affords $\Theta_{CW} = -18.5$ K $\equiv -12.89$ cm^{-1}, which fixes the sum $J_{rr} + J_{CR}$ in our analysis discussed below with regards to the parameterization of the magnetic Hamiltonian. We note that this implies, based on the sign of the sum of the exchange constants, that the dominant exchange is antiferromagnetic.

Neutron scattering

Neutron spectroscopy results from LET (ISIS) are presented in Fig. 3. Fig. 3(a and b) illustrate the background corrected data at $T = 2$ K using the detailed balance analysis to extract $S(\vec{Q},\omega)$ for incident energies of $E_i = 12$ and 3 meV. In both panels, we have corrected for a phonon background using the extracted $S(\vec{Q},\omega)$ at $T = 80$ K by,

$$\begin{aligned} S(\vec{Q},\omega,T=2\,\mathrm{K})_{mag} &= S(\vec{Q},\omega,T=2\,\mathrm{K}) - S(\vec{Q},\omega,T=2\,\mathrm{K})_{phonon} \\ &= S(\vec{Q},\omega,T=2\,\mathrm{K}) - S(\vec{Q},\omega,T=80\,\mathrm{K}) \\ &\quad \times (1 - \exp -\omega/k_B T = 80\,\mathrm{K}) \end{aligned}$$

thereby estimating the purely magnetic cross section at $T = 2$ K. The scattering in Fig. 3a and b displays a weak peak at ~6 meV and strong scattering at low energies below ~3 meV. This is further displayed in Fig. 3c which plots the momentum integrated intensity as a function of energy for the two experimental configurations. For comparison, the data are normalized to agree at low energy transfers. The dashed line is discussed below in terms of a parameterization of the microscopic magnetic Hamiltonian.

Parameterization

To parameterize the results, we have combined the first principles DFT results with the thermodynamic magnetic susceptibility to constrain excitonic calculations for the neutron spectroscopy results.

The methodology we have used involves first fitting the high temperature magnetic susceptibility to obtain a Curie–

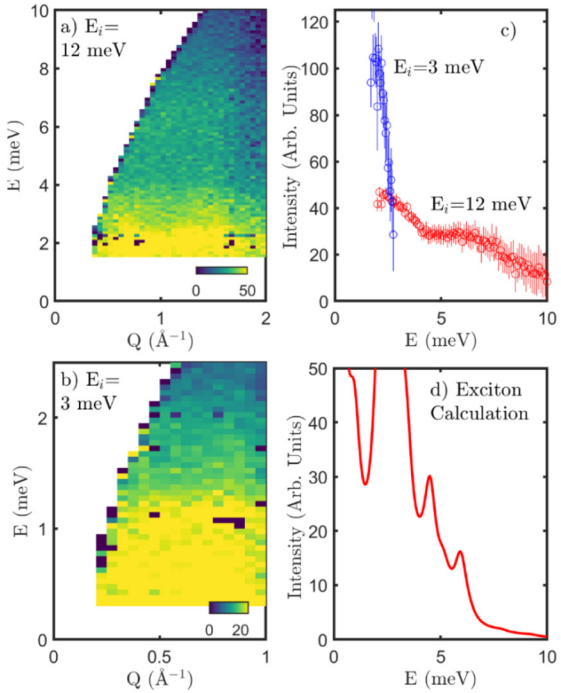

Fig. 3 Summary of the neutron spectroscopy results taken on LET at T = 2 K with background and phonon corrected data displayed in (a) E_i = 12 meV and (b) E_i = 3 meV. (c) Momentum integrated intensity normalized at E = 2.5 meV for E_i = 3 meV ($\vec{Q} = [0,1]$ Å^{-1}) and E_i = 12 meV ($\vec{Q} = [0,2]$ Å^{-1}). (d) Excitonic calculation described in the main text constrained by first principles calculations.

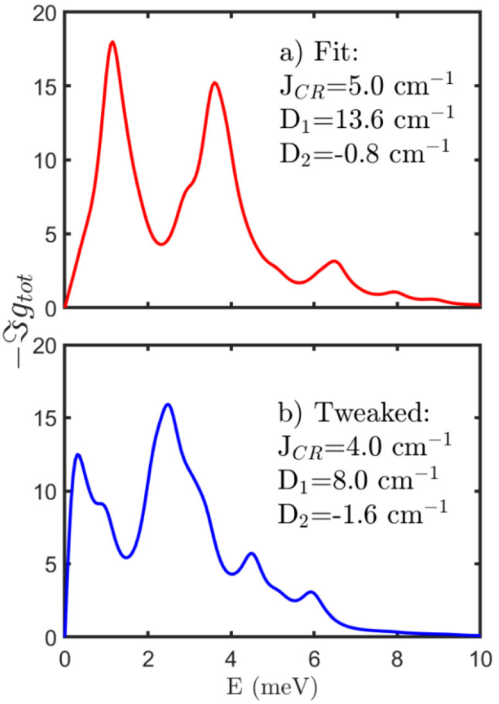

Fig. 4 Excitonic calculations constrained by first principles calculations described in the text. (a) Least squares fit to the high energy data taken with E_i = 12 meV. (b) Tweaked values to produce a weak peak near 6 meV and strong low-energy scattering as qualitatively observed in the neutron inelastic response. The variation of parameters is a measure of the underlying error bar in the determined values.

Weiss constant thereby fixing the sum of the two exchange constants J_{rr} and J_{CR} with the signs of these exchange constants fixed through the DFT first principles calculations described above. Applying the results from neutron spectroscopy and our excitonic calculations described above, we then parameterize the two excitations observed through varying the anisotropy parameters, also guided by first principles calculations.

This parameterization was done by performing a least squares fit to the E_i = 12 meV data illustrated in Fig. 3. The results of this are shown in Fig. 4a. This fit produces a weak high energy peak as found in the data, however it fails to capture the significant intensity present at low-energies found in the E_i = 3 meV data in Fig. 3b and c. The parameters were then varied to bring the spectra down to lower energies while preserving a weak peak at ~6 meV and keeping the values consistent with DFT estimates and within the constraints set by the high temperature Curie Weiss temperature (Θ_{CW}). Based on this iterative procedure, we derive the following parameters for the microscopic magnetic Hamiltonian, J_{cr} = +4.0 cm^{-1}, J_{rr} = −5.66 cm^{-1}, D_1 = +8.0 cm^{-1} and D_2 = −1.6 cm^{-1}. The results of this analysis are displayed in Fig. 3d and 4b with differences in values from Fig. 4(a) and (b) representative of the underlying error bars for the parameterized values. These are in good agreement with fits of the susceptibility/magnetization data and theoretical calculations.

Conclusions

Despite several [Ni$^{II}_7$] Anderson wheels being previously reported, there has to date been no consensus on the magnitude and sign of the pairwise magnetic exchange interactions present, nor on the sign/magnitude of the single ion anisotropies of the constituent metal centres. In order to address this we have reported the synthesis, structure and characterization of the Anderson wheel [Ni$_7$(hmp)$_{7.55}$(pic)$_{4.45}$](ClO$_4$)$_2$·6MeOH (**1**·6MeOH) through a combination of first principles calculations, magnetic susceptibility and magnetisation measurements, and neutron scattering. To the best of our knowledge this combination of techniques is employed for the first time on any [Ni$_7$] species. To consistently describe the magnetic parameters and neutron response we applied an excitonic formalism using a Green's function response theory. The combined conclusions from these techniques and data analysis are: (a) the magnetic exchange between the central Ni ion and the ring Ni ions is ferromagnetic, (b) the magnetic exchange between the ring Ni ions is antiferromagnetic, (c) the central Ni ion possesses easy plane anisotropy, (d) the ring Ni ions possess easy axis anisotropy. Given the structural similarity between **1** and other [Ni$_7$] in the literature, we believe these conclusions may also be valid more generally.

Author contributions

EHP and LRBW performed the synthesis, and collected the PXRD/SQUID data; GSN collected and solved the single crystal XRD data; MKS performed the theoretical calculations; JS fitted the susceptibility and magnetisation data; JRS, VGS, RAE, HL and CS collected/analysed the neutron scattering data; EKB conceived the idea. All authors contributed to writing and editing the manuscript.

Conflicts of interest

There are no conflicts to declare.

Acknowledgements

We thank the European Union Horizon 2020 Research and Innovation Programme under the Marie Skłodowska-Curie grant agreement no. 832488 (MKS).

References

1 K. O. Joung, C. J. O'Connor, E. Sinn and R. L. Carlin, Structural and magnetic properties of dimeric di-.mu.-chloro-tetrakis(ethylenediamine)dinickel(II) chloride, *Inorg. Chem.*, 1979, **18**, 804–808.

2 (*a*) K. E. Andrew and A. B. Blake, The crystal structure and magnetic properties of tetra-μ_3-methoxytetrakis[salicylaldehydato(ethanol)nickel(II)], *J. Chem. Soc. A*, 1969, 1456; J. A. Barnes and W. E. Hatfield, Low-temperature magnetic susceptibility of tetra-.mu.3-methoxy-tetrakis[salicylaldehydato(ethanol)nickel(II)], a complex with a positive exchange coupling constant, *Inorg. Chem.*, 1971, **10**, 2355–2357; M. A. Halcrow, J.-S. Sun and J. C, Huffman and G. Chrsitou, Structural and Magnetic Properties of [Ni4(.mu.3-OMe)4(dbm)4(MeOH)4] and [Ni4(.eta.1,.mu.3-N3)4(dbm)4(EtOH)4]. Magnetostructural Correlations for [Ni4X4]4+ Cubane Complexes, *Inorg. Chem.*, 1995, **34**, 4167–4177.

3 H. Andres, R. Basler, A. J. Blake, C. Cadiou, G. Chaboussant, C. M. Grant, H.-U. Güdel, M. Murrie, S. Parsons, C. Paulsen, F. Semadini, V. Villar, W. Wernsdorfer and R. E. P. Winpenny, Studies of a Nickel-Based Single-Molecule Magnet, *Chem. – Eur. J.*, 2002, **8**, 4867–4876.

4 (*a*) R. Ruamps, R. Maurice, L. Batchelor, M. Boggio-Pasqua, R. Guillot, A. L. Barra, J. Liu, E.-E. Bendeif, S. Pillet, S. Hill, T. Mallah and N. Guihéry, Giant Ising-Type Magnetic Anisotropy in Trigonal Bipyramidal Ni(II) Complexes: Experiment and Theory, *J. Am. Chem. Soc.*, 2013, **135**, 3017–3026; (*b*) K. E. R. Marriott, L. Bhaskaran, C. Wilson, M. Medarde, S. T. Ochsenbein, S. Hill and M. Murrie, *Chem. Sci.*, 2015, **6**, 6823–6828; (*c*) G. A. Craig, A. Sarkar, C. H. Woodall, M. A. Hay, K. E. R. Marriott, K. V. Kamenev, S. A. Moggach, E. K. Brechin, S. Parsons, G. Rajaraman and M. Murrie, Pushing the limits of magnetic anisotropy in trigonal bipyramidal Ni(II), *Chem. Sci.*, 2018, **9**, 1551–1559.

5 (*a*) K. Bader, S. H. Schlindwein, D. Gudat and J. van Slageren, Molecular qubits based on potentially nuclear-spin-free nickel ions, *Phys. Chem. Chem. Phys.*, 2017, **19**, 2525–2529; (*b*) M. K. Wojnar, M. K. Wojnar, D. W. Laorenza, R. D. Schaller and D. E. Freedman, Nickel(II) Metal Complexes as Optically Addressable Qubit Candidates, *J. Am. Chem. Soc.*, 2020, **142**, 14826–14830.

6 E.-C. Yang, W. Wernsdorfer, S. Hill, R. S. Edwards, M. Nakano, S. Maccagnano, L. N. Zakharov, A. L. Rheingold, G. Christou and D. N. Hendrickson, Exchange bias in Ni_4 single-molecule magnets, *Polyhedron*, 2003, **22**, 1727–1733.

7 N. Kirchner, J. van Slageren, B. Tsukerblat, O. Waldmann and M. Dressel, Antisymmetric exchange interactions in Ni_4 clusters, *Phys. Rev. B: Condens. Matter Mater. Phys.*, 2008, **78**, 094426.

8 Y. Chen, M. D. Ashkezari, C. A. Collett, R. A. Allão Cassaro, F. Troiani, P. M. Lahti and J. R. Friedman, Observation of Tunneling-Assisted Highly Forbidden Single-Photon Transitions in a Ni_4 Single-Molecule Magnet, *Phys. Rev. Lett.*, 2016, **117**, 187202.

9 C. A. Collett, R. A. Allão Cassaro and J. R. Friedman, Precision ESR Measurements of Transverse Anisotropy in the Single-molecule Magnet Ni_4, *Phys. Rev. B*, 2016, **94**, 220402.

10 B. C. Sheehan, R. Kwark, C. A. Collett, T. A. Costa, R. A. Allão Cassaro and J. R. Friedman, Direct spectroscopic observation of Berry-phase interference in the Ni_4 single-molecule magnet, *Phys. Rev. B*, 2020, **102**, 224428.

11 A. L. Dearden, S. Parsons and R. E. P. Winpenny, Synthesis, Structure, and Preliminary Magnetic Studies of a Ni_{24} Wheel, *Angew. Chem., Int. Ed.*, 2001, **40**, 151–154.

12 G. Aromí, S. Parsons, W. Wernsdorfer, E. K. Brechin and E. J. L. McInnes, Synthesis, structure and magnetic properties of a decametallic Ni single-molecule magnet, *Chem. Commun.*, 2005, 5038–5040.

13 M. I. Gonzalez, A. B. Turkiewicz, L. E. Darago, J. Oktawiec, K. Bustillo, F. Grandjean, G. J. Long and J. R. Long, Confinement of atomically defined metal halide sheets in a metal-organic framework, *Nature*, 2020, **577**, 64–68.

14 J. N. Behera and C. N. R. Rao, A Ni^{2+} (S = 1) Kagome Compound Templated by 1,8-Diazacubane, *J. Am. Chem. Soc.*, 2006, **128**, 9334–9335.

15 H. W. L. Fraser, G. S. Nichol, D. Uhrín, U. G. Nielsen, M. Evangelisti, J. Schnack and E. K. Brechin, Order in disorder: solution and solid-state studies of $[M^{III}{}_2M^{II}{}_5]$ wheels (M^{III} = Cr, Al; MII = Ni, Zn), *Dalton Trans.*, 2018, **47**, 11834–11842.

16 (*a*) J. S. Anderson, Constitution of the Poly-acids, *Nature*, 1937, 850; (*b*) H. T. Evans, The crystal structures of ammonium and potassium molybdotellurate, *J. Am. Chem. Soc.*, 1948, **70**, 1291–1292.

17 A. Blazevic and A. Rompel, The Anderson–Evans polyoxometalate: From inorganic building blocks *via* hybrid organic–inorganic structures to tomorrows "Bio-POM", *Coord. Chem. Rev.*, 2016, **307**, 42–64.
18 H. W. L. Fraser, G. S. Nichol, A. Baldansuren, E. J. L. McInnes and E. K. Brechin, Cages on a plane: a structural matrix for molecular 'sheets', *Dalton Trans.*, 2018, **47**, 15530–15537.
19 F. H. Allen, The Cambridge Structural Database: a quarter of a million crystal structures and rising, *Acta Crystallogr., Sect. B: Struct. Sci.*, 2002, **58**, 380–388.
20 S. T. Meally, G. Karotsis, E. K. Brechin, G. S. Papaefstathiou, P. W. Dunne, P. McArdle and L. F. Jones, A family of double-bowl pseudometallocalix[6] arene discs, *CrystEngComm*, 2010, **12**, 59–63.
21 J. Zhang, P. Teo, R. Pattacini, A. Kermagoret, R. Welter, G. Rogez, T. S. A. Hor and P. Braunstein, Structural Effects of Sodium Cations in Polynuclear, Multicubane-Type Mixed Na–Ni Complexes, *Angew. Chem., Int. Ed.*, 2010, **49**, 4443–4446.
22 S. T. Meally, C. McDonald, G. Karotsis, G. S. Papaefstathiou, E. K. Brechin, P. W. Dunne, P. McArdle, N. P. Power and L. F. Jones, A family of double-bowl pseudo metallocalix[6]arene discs, *Dalton Trans.*, 2010, **39**, 4809–4816.
23 W. L. Leong and J. J. Vittal, Alkali metal ion directed self-assembled Ni(II) molecular clusters, *New J. Chem.*, 2010, **34**, 2145–2152.
24 S. H. Zhang, N. Li, C. M. Ge, C. Feng and L. F. Ma, Structures and magnetism of $\{Ni_2Na_2\}$, $\{Ni_4\}$ and $\{Ni_6^{II}Ni^{III}\}$ 2-hydroxy-3-alkoxy-benzaldehyde clusters, *Dalton Trans.*, 2011, **40**, 3000–3007.
25 L. Q. Wei, K. Zhang, Y. C. Feng, Y. H. Wang, M. H. Zeng and M. Kurmoo, Microwave versus Traditional Solvothermal Synthesis of Ni_7^{II} Discs: Effect of Ligand on Exchange Reaction in Solution Studied by Electrospray Ionization-Mass Spectroscopy and Magnetic Properties, *Inorg. Chem.*, 2011, **50**, 7274–7283.
26 C. X. Ding, C. Gao, S. Ng, B. W. Wang and Y. S. Xie, Polynuclear Complexes with Alkoxo and Phenoxo Bridges from In Situ Generated Hydroxy-Rich Schiff Base Ligands: Syntheses, Structures, and Magnetic Properties, *Chem. – Eur. J.*, 2013, **19**, 9961–9972.
27 A. K. Ghosh, A. Bauza, V. Bertolasi, A. Frontera and D. Ray, Dinuclear and heptanuclear nickel(II) complexes: Anion coordination induced ligand arm hydrolysis and aggregation around a nickel(II) core, *Polyhedron*, 2013, **53**, 32–39.
28 Q. P. Huang, S. H. Zhang, H. Y. Zhang, G. Li and M. C. Wu, Microwave-Assisted Synthesis, Structure and Properties of a Nano-Double-Bowl-Like Heptanuclear Nickel(II) Cluster, *J. Cluster Sci.*, 2014, **25**, 1489–1499.
29 L. Yang, Q. P. Huang, C. L. Zhang, R. X. Zhao and S. H. Zhang, Two disc-like heptanuclear clusters based on Schiff base: syntheses, structure and magnetic properties, *Supramol. Chem.*, 2014, **26**, 81–87.
30 D. I. Alexandropoulos, L. Cunha-Silva, A. Escuer and T. C. Stamatatos, New Classes of Ferromagnetic Materials with Exclusively End-on Azido Bridges: From Single-Molecule Magnets to 2 D Molecule-Based Magnets, *Chem. – Eur. J.*, 2014, **20**, 13860–13864.
31 S. H. Zhang, R. X. Zhao, G. Li, H. Y. Zhang, C. L. Zhang and G. Muller, Structural variation from heterometallic heptanuclear or heptanuclear to cubane clusters based on 2-hydroxy-3-ethoxy-benzaldehyde: effects of pH and temperature, *RSC Adv.*, 2014, **4**, 54837–54846.
32 X. Yu, H. Pu and L. Y. Qing, Microwave Assisted Synthesis, and Structure of a Co-Crystal Nickel Complex with 2-ethoxy-6-methyliminomethyl-phenol, *Mol. Cryst. Liq. Cryst.*, 2015, **607**, 242–249.
33 Y. Xiao, Y. Q. Liu, G. Li and P. Huang, Microwave-assisted synthesis, structure and properties of a co-crystal compound with 2-ethoxy-6-methyliminomethyl-phenol, *Supramol. Chem.*, 2015, **27**, 161–166.
34 S. H. Zhang, G. Li, H. Y. Zhang and H. P. Li, Microwave-assisted synthesis, structure and property of a spin-glass heptanuclear nickel cluster with 2-iminomethyl-6-methoxy-phenol, *Z. Kristallogr.*, 2015, **230**, 479–484.
35 Y. Xiao, Y. Qin, M. Yi and Y. Zhu, A Disc-Like Heptanuclear Nickel Cluster Based on Schiff Base: Synthesis, Structure, Magnetic Properties and Hirshfeld Surface Analysis, *J. Cluster Sci.*, 2016, **27**, 2013–2023.
36 F. Kobayashi, R. Ohtani, S. Teraoka, W. Kosaka, H. Miyasaka, Y. J. Zhang, L. F. Lindoy, S. Hayami and M. Nakamura, Syntheses, structures and magnetic properties of tetranuclear cubane-type and heptanuclear wheel-type nickel(II) complexes with 3-methoxysalicylic acid derivatives, *Dalton Trans.*, 2017, **46**, 8555–8561.
37 R. Gheorghe, G. A. Ionita, C. Maxim, A. Caneschi, L. Sorace and M. Andruh, Aggregation of heptanuclear $[M^{II}_7]$ (M = Co, Ni, Zn) clusters by a Schiff-base ligand derived from o-vanillin: Synthesis, crystal structures and magnetic properties, *Polyhedron*, 2019, **171**, 269–278.
38 T. Zhang, L. L. Zhang, C. X. Ji, S. Ma, Y. X. Sun, J. P. Zhao and F. C. Log, Construction of Designated Heptanuclear Metal 8-hydroxyquinolates with Different Ions and Auxiliary Coligands, *Cryst. Growth Des.*, 2019, **19**, 3372–3378.
39 G. M. Sheldrick, SHELXT - Integrated space-group and crystal-structure determination, *Acta Crystallogr.*, 2015, **C71**, 3–8.
40 G. M. Sheldrick, SHELXT - Integrated space-group and crystal-structure determination, *Acta Crystallogr.*, 2015, **A71**, 3–8.
41 O. V. Dolomanov, L. J. Bourhis, R. J. Gildea, J. A. K. Howard and H. Puschmann, OLEX2: a complete structure solution, refinement and analysis program, *J. Appl. Crystallogr.*, 2009, **42**, 339–341.
42 M. J. Frisch, G. W. Trucks, H. B. Schlegel, G. E. Scuseria, M. A. Robb, J. R. Cheeseman, G. Scalmani, V. Barone, G. A. Petersson, H. Nakatsuji, X. Li, M. Caricato, A. V. Marenich, J. Bloino, B. G. Janesko, R. Gomperts,

B. Mennucci, H. P. Hratchian, J. V. Ortiz, A. F. Izmaylov, J. L. Sonnenberg, D. Williams-Young, F. Ding, F. Lipparini, F. Egidi, J. Goings, B. Peng, A. Petrone, T. Henderson, D. Ranasinghe, V. G. Zakrzewski, J. Gao, N. Rega, G. Zheng, W. Liang, M. Hada, M. Ehara, K. Toyota, R. Fukuda, J. Hasegawa, M. Ishida, T. Nakajima, Y. Honda, O. Kitao, H. Nakai, T. Vreven, K. Throssell, J. A. Montgomery Jr., J. E. Peralta, F. Ogliaro, M. J. Bearpark, J. J. Heyd, E. N. Brothers, K. N. Kudin, V. N. Staroverov, T. A. Keith, R. Kobayashi, J. Normand, K. Raghavachari, A. P. Rendell, J. C. Burant, S. S. Iyengar, J. Tomasi, M. Cossi, J. M. Millam, M. Klene, C. Adamo, R. Cammi, J. W. Ochterski, R. L. Martin, K. Morokuma, O. Farkas, J. B. Foresman and D. J. Fox, Gaussian, Inc., Wallingford CT, 2016.

43 (*a*) C. Lee, W. Yang and R. G. Parr, Development of the Colle-Salvetti correlation-energy formula into a functional of the electron density, *Phys. Rev. B: Condens. Matter*, 1988, **37**, 785; (*b*) A. D. Becke, Density–functional thermochemistry. III. The role of exact exchange, *J. Chem. Phys.*, 1993, **98**, 5648–5652; (*c*) A. D. Becke, A new mixing of Hartree–Fock and local density–functional theories, *J. Chem. Phys.*, 1993, **98**, 1372–1377; (*d*) P. J. Stephens, F. J. Devlin, C. F. Chabalowski and M. J. Frisch, Ab Initio Calculation of Vibrational Absorption and Circular Dichroism Spectra Using Density Functional Force Fields, *J. Phys. Chem.*, 1994, **98**, 11623–11627.

44 (*a*) A. Schäfer, H. Horn and R. Ahlrichs, Fully optimized contracted Gaussian basis sets for atoms Li to Kr, *J. Chem. Phys.*, 1992, **97**, 2571–2577; (*b*) A. Schäfer, C. Huber and R. Ahlrichs, Fully optimized contracted Gaussian basis sets of triple zeta valence quality for atoms Li to Kr, *J. Chem. Phys.*, 1994, **100**, 5829–5835; (*c*) G. E. Scuseria and H. F. Schaefer III, Is coupled cluster singles and doubles (CCSD) more computationally intensive than quadratic configuration interaction (QCISD)?, *J. Chem. Phys.*, 1989, **90**, 3700–3703.

45 P. C. Hariharan and J. A. Pople, The influence of polarization functions on molecular orbital hydrogenation energies, *Theor. Chim. Acta*, 1973, **28**, 213–222.

46 (*a*) L. Noodleman and D. A. Case, Density-Functional Theory of Spin Polarization and Spin Coupling in Iron—Sulfur Clusters, *Adv. Inorg. Chem.*, 1992, **38**, 423–458; (*b*) L. Noodleman and E. R. Davidson, Ligand spin polarization and antiferromagnetic coupling in transition metal dimers, *Chem. Phys.*, 1986, **109**, 131–143; (*c*) L. Noodleman, Valence bond description of antiferromagnetic coupling in transition metal dimers, *J. Chem. Phys.*, 1981, **74**, 5737–5743; (*d*) L. Noodleman and J. G. Norman, The Xα valence bond theory of weak electronic coupling. Application to the low–lying states of $Mo_2Cl_8^{4-}$, *J. Chem. Phys.*, 1979, **70**, 4903–4906.

47 F. Neese, The ORCA program system, *Wiley Interdiscip. Rev.: Comput. Mol. Sci.*, 2012, 2, 73–78.

48 (*a*) K. Eichkorn, O. Treutler, H. Öhm, M. Häser and R. Ahlrichs, Auxiliary basis sets to approximate Coulomb potentials, *Chem. Phys. Lett.*, 1995, **242**, 652–660; (*b*) K. Eichkorn, F. Weigend, O. Treutler and R. Ahlrichs, Auxiliary basis sets for main row atoms and transition metals and their use to approximate Coulomb potentials, *Theor. Chem. Acc.*, 1997, **97**, 119–124; (*c*) F. Weigend and R. Ahlrichs, Balanced basis sets of split valence, triple zeta valence and quadruple zeta valence quality for H to Rn: Design and assessment of accuracy, *Phys. Chem. Chem. Phys.*, 2005, **7**, 3297–3305; (*d*) F. Neese, Importance of Direct Spin–Spin Coupling and Spin-Flip Excitations for the Zero-Field Splittings of Transition Metal Complexes: A Case Study, *J. Am. Chem. Soc.*, 2006, **128**, 10213–10222; (*e*) F. Neese and E. I. Solomon, Calculation of Zero-Field Splittings, g-Values, and the Relativistic Nephelauxetic Effect in Transition Metal Complexes. Application to High-Spin Ferric Complexes, *Inorg. Chem.*, 1998, **37**, 6568–6582; (*f*) D. Maganas, S. Sottini, P. Kyritsis, E. J. J. Groenen and F. Neese, Theoretical Analysis of the Spin Hamiltonian Parameters in $Co^{(II)}S_4$ Complexes, Using Density Functional Theory and Correlated ab initio Methods, *Inorg. Chem.*, 2011, **50**, 8741–8754; (*g*) E. Cremades and E. Ruiz, Mononuclear FeII Single-Molecule Magnets: A Theoretical Approach, *Inorg. Chem.*, 2011, **50**, 4016–4020; (*h*) S. Ye and F. Neese, How Do Heavier Halide Ligands Affect the Signs and Magnitudes of the Zero-Field Splittings in Halogenonickel(II) Scorpionate Complexes? A Theoretical Investigation Coupled to Ligand-Field Analysis, *J. Chem. Theory Comput.*, 2012, **8**, 2344–2351; (*i*) R. Maurice, L. Vendier and J.-P. Costes, Magnetic Anisotropy in Ni^{II}–Y^{III} Binuclear Complexes: On the Importance of Both the First Coordination Sphere of the Ni^{II} Ion and the Y^{III} Ion Belonging to the Second Coordination Sphere, *Inorg. Chem.*, 2011, **50**, 11075–11081.

49 (*a*) C. Angeli, R. Cimiraglia, S. Evangelisti, T. Leininger and J.-P. Malrieu, ntroduction of n-electron valence states for multireference perturbation theory, *J. Chem. Phys.*, 2001, **114**, 10252–10264; (*b*) C. Angeli, R. Cimiraglia and J.-P. Malrieu, n-electron valence state perturbation theory: A spinless formulation and an efficient implementation of the strongly contracted and of the partially contracted variants, *J. Chem. Phys.*, 2002, **117**, 9138–9153; (*c*) C. Angeli, R. Cimiraglia and J.-P. Malrieu, N-electron valence state perturbation theory: a fast implementation of the strongly contracted variant, *Chem. Phys. Lett.*, 2001, **350**, 297–305.

50 (*a*) T. Hong, M. Kenzelmann, M. M. Turnbull, C. P. Landee, B. D. Lewis, K. P. Schmidt, G. S. Uhrig, Y. Qiu, C. Broholm and D. Reich, Neutron scattering from a coordination polymer quantum paramagnet, *Phys. Rev. B: Condens. Matter Mater. Phys.*, 2006, **74**, 094434; (*b*) C. Stock, E. E. Rodriguez and M. A. Green, Spin fluctuations and superconductivity in powders of $Fe_{1+x}Te_{0.7}Se_{0.3}$ as a function of interstitial iron concentration, *Phys. Rev. B: Condens. Matter Mater. Phys.*, 2012, **85**, 094507.

51 (*a*) M. K. Singh and G. Rajaraman, Theoretical Studies on Hexanuclear $[M_3(\mu_3\text{-O/OH})]_2$ (M = Fe(III), Mn(III), and Ni(II) Clusters: Magnetic Exchange, Magnetic Anisotropy, and Magneto-Structural Correlations, *Inorg. Chem.*, 2019, **58**,

3175–3188; (*b*) M. A. Halcrow, J.-S. Sun, J. C. Huffman and G. Christou, Structural and Magnetic Properties of $[Ni_4(mu_3\text{-}OMe)_4(d\ bm)_4(MeOH)_4]$ and $[Ni_4(eta,mu_3\text{-}N_3)_4(dbm)_4(EtOH)_4]$. Magnetostructural Correlations for $[Ni_4X_4]^{4+}$ Cubane Complexes, *Inorg. Chem.*, 1995, **34**, 4167–4177; (*c*) K. K. Nanda, L. K. Thompson, J. N. Bridson and K. Nag, Linear dependence of spin exchange coupling constant on bridge angle in phenoxy-bridged dinickel(II) complexes, *J. Chem. Soc., Chem. Commun.*, 1994, 1337–1338; (*d*) L. Ballester, E. Coronado, A. Gutierrez, A. Monge, M. F. Perpinan, E. Pinilla and T. Rico, Studies on the reactivity of S,N-derivatives of nickel with N-donor bases. Crystal structure and magnetic properties of the cubane cluster tetrakis(.mu.-hydroxo)tetrakis(.mu.-1,3-thiazolidine-2-thionato)tetrakis(pyridine)tetranickel(II)-dipyridine, *Inorg. Chem.*, 1992, **31**, 2053–2056; (*e*) E. Agapaki, M. K. Singh, A. B. Canaj, G. S. Nichol, J. Schnack and E. K. Brechin, A graceful break-up: serendipitous self-assembly of a ferromagnetically coupled $[Ni^{II}_{14}]$ wheel, *Chem. Commun.*, 2022, **58**, 9088–9091.

52 (*a*) A. Sarkar, S. Dey and G. Rajaraman, Role of Coordination Number and Geometry in Controlling the Magnetic Anisotropy in Fe^{II}, Co^{II}, and Ni^{II} Single-Ion Magnets, *Chem. – Eur. J.*, 2020, **26**, 14036–14058; (*b*) S. K. Singh, T. Gupta, P. Badkur and G. Rajaraman, Magnetic Anisotropy of Mononuclear Ni^{II} Complexes: On the Importance of Structural Diversity and the Structural Distortions, *Chem. – Eur. J.*, 2014, **20**, 10305; (*c*) D. Lomjanský, C. Rajnák, J. Titiš, J. Moncoľ and R. Boča, Study of zero-field splitting in Ni(II) complexes with near octahedral geometry, *Inorg. Chim. Acta*, 2019, **491**, 138–146; (*d*) T. Laluhová, J. Titiš, C. Rajnák, J. Moncoľ and R. Boča, Magnetism of pseudohalide Ni(II) complexes containing 4-methylpyridine ligands, *Polyhedron*, 2022, **227**, 116135.

53 P. M. Sarte, M. Songvilay, E. Pachoud, R. A. Ewings, C. D. Frost, D. Prabhakaran, K. H. Hong, A. J. Browne, Z. Yamani, J. P. Attfield, E. E. Rodriguez, S. D. Wilson and C. Stock, Spin-orbit excitons in CoO, *Phys. Rev. B*, 2019, **100**, 075143.

54 P. M. Sarte, C. Stock, B. R. Ortiz, K. H. Hong and S. D. Wilson, Van Vleck excitons in Ca_2RuO_4, *Phys. Rev. B*, 2020, **102**, 245119.

55 H. Lane, M. Songvilay, R. A. Ewings and C. Stock, Excitonic transverse and amplitude fluctuations in noncollinear and charge-ordered $RbFe^{2+}Fe^{3+}F_6$, *Phys. Rev. B*, 2022, **106**, 054431.

56 H. Lane, E. E. Rodriguez, H. C. Walker, C. Niedermayer, U. Stuhr, R. I. Bewley, D. J. Voneshen, M. A. Green, J. A. Rodriguez-Rivera, P. Fouquet, S.-W. Cheong, J. P. Attfield, R. A. Ewings and C. Stock, Metastable antiphase boundary ordering in $CaFe_2O_4$, *Phys. Rev. B*, 2021, **104**, 104404.

57 W. J. L. Buyers, T. M. Holden and A. Perreault, Temperature dependence of magnetic excitations in singlet-ground-state systems. II. Excited-state spin waves near the Curie temperature in Pr_3Tl, *Phys. Rev. B: Solid State*, 1975, **11**, 266.